PHYSICAL REVIEW D **73,** 034007 (2006)

Bound state effects in transverse momentum parton distributions

F. K. Diakonos,* G. D. Galanopoulos, and X. N. Maintas
Department of Physics, University of Athens, GR-15771 Athens, Greece
(Received 14 October 2005; published 8 February 2006)

We derive a nonperturbative transverse momentum distribution for partons using a potential model to describe the quark-quark interaction inside the proton. We use this distribution in the calculation of the differential cross section of π^0 production for intermediate transverse momentum values in $p-p$ collisions at high energies. Assuming a variable string tension constant for the quark-quark potential we obtain a very good description of the experimental data at different energies. The corresponding values of the mean transverse momentum of the partons are essentially lower than those obtained using a Gaussian transverse momentum parton distribution. Using the same approach we can also describe the proton production data in the Chicago-Princeton experiment. Our analysis indicates that bound state effects may be important for the description of the experimental data in proton-proton collisions.

DOI: 10.1103/PhysRevD.73.034007 PACS numbers: 13.85.Ni, 12.39.Jh

I. INTRODUCTION

During the last decades the tests of perturbative QCD have been focused on the experimental [1–16] and theoretical study [17–27] of hard processes like direct photon and π^0 production with large transverse momentum in pp, pA, and AA collisions. These processes offer a unique possibility to test the parton distribution functions (PDF) inside the proton as well as the parton fragmentation functions (PFF) determined by deep inelastic scattering or e^+e^- annihilation. In particular the good understanding of the pp data is the prerequisite for any attempt to extract new physics, related to the formation of a quark-gluon plasma phase, from the pA and AA data. Extensive studies of the π (or γ) production in pp collisions have shown that the transverse momentum distribution $g(k_T)$ of the partons inside the proton has to be taken into account for a successful description of the observed p_T spectrum [21–24]. In all these investigations one assumes a Gaussian form for $g(k_T)$. A new nonperturbative parameter is introduced through this approach: the mean intrinsic transverse momentum $\langle k_T\rangle$ of the partons. Although the data of some experiments concerning hadron production at large p_T [21,22] could be explained with relatively small $\langle k_T\rangle$ values ($\approx$ 0.3–0.5 GeV), compatible with the Heisenberg uncertainty relation for partons inside the proton, there are a number of other processes leading to a large mean transverse momentum ($\langle k_T\rangle \approx$ 1–4 GeV), depending on Q^2, for a description of the corresponding experimental data. Such a value of $\langle k_T\rangle$ is too high and cannot be explained as an internal structure of the proton [24]. However, as mentioned by several authors [20–22] the form of $g(k_T)$ can influence significantly the value of $\langle k_T\rangle$ as well as its p_T dependence. In the present work we derive a transverse momentum distribution for the partons inside the proton using a potential quark model which has successfully been used to describe the spectra of mesonic [28,29] and baryonic [29,30] bound states in the past. Following [30,31] we investigate the three-body quantum mechanical bound state problem solving numerically the Schrödinger equation and obtaining the single particle transverse momentum distribution for the constituent parton. Our main assumption is that intrinsic transverse momentum effects are not influenced by the Lorentz boost along the beam axis and therefore could be treated within a nonrelativistic approach. We use the derived distribution to fit experimental data for the $pp \rightarrow \pi^0 + X$ and $pp \rightarrow p + X$ process. In particular we investigate the measurements for the p_T spectrum of the outcoming π^0 in four experiments performed at different center of mass energies. It turns out that a relatively low mean transverse momentum $\langle k_T\rangle (\approx O(300\ \mathrm{MeV}))$, compatible with intrinsic dynamics inside the proton, for the initial partons is sufficient in order to fit perfectly the experimental data. A smooth dependence of $\langle k_T\rangle$ on p_T, which within our approach is induced by a corresponding variation of the string tension in the quark-quark potential, is required. Our analysis shows that the k_T distribution of the constituent partons can be strongly influenced by three-body effects and the form of the confining potential which have to be taken into account in order to describe correctly the experimental data concerning the pion production in pp collisions. The paper is organized as follows: in Sec. II we present the parton model differential cross section as well as the corresponding kinematics for the π^0 production in pp collisions. In Sec. III we derive the intrinsic transverse momentum distribution for the partons inside the proton using the quark potential model of [28]. In Sec. IV we present our numerical results concerning the description of the data of four different experiments [1,6,7,16] as well as the corresponding dependence $\langle k_T(p_T)\rangle$. Finally, in Sec. V we summarize our study and we discuss possible extensions of the present analysis.

*Electronic address: fdiakono@phys.uoa.gr

II. THE $pp \to \pi^0 + X$ CROSS SECTION

The differential cross section for the production of hadron h in pp collisions within the perturbative QCD improved parton model is given by

$$E_\pi \frac{d\sigma}{d^3p}(pp \to h + X) = K \sum_{abcd} \int dx_a dx_b f_{a/p}(x_a, Q^2) \times f_{b/p}(x_b, Q^2) \frac{d\sigma}{d\hat{t}}(ab \to cd) \times \frac{D_{h/c}(z_c, \tilde{Q}^2)}{\pi z_c}. \quad (1)$$

The convolution appearing in Eq. (1) is based on the factorization theorem which allows for the absorption of higher order mass singularities into the uncalculated portions of the partonic distribution and fragmentation functions [17,22,32]. In Eq. (1) $f_{i/p}(x_i, Q^2)$ $(i = a, b)$ are the parton distribution functions for the colliding partons a and b in the interacting protons as functions of longitudinal momentum fraction x_i at scale Q. The hard scattering cross section $\frac{d\sigma}{d\hat{t}}$ describes the partonic subprocess $ab \to cd$. The parton fragmentation function $D_{h/c}(z_c, \tilde{Q}^2)$ gives the probability for parton c to fragment into hadron h with momentum fraction z_c at scale $\tilde{Q}$. Finally the factor K can be adjusted to the value $K \approx 2$ in order to take into account higher order corrections in the partonic subprocesses. In the following analysis we will use different choices for the factorization scales Q, $\tilde{Q}$. In addition we will use alternatively the values $K = 1$ and $K = 2$ for the factor K corresponding to leading order or higher order approximation to the partonic cross sections, respectively. Assuming that the distribution of the partonic transverse momentum is independent of the longitudinal momentum fraction x and the scale Q permits us to use the widely applied in the literature factorization ansatz and include parton transverse momentum effects in our approach through the replacement [21,22,33]:

$$dx_i f_{i/p}(x_i, Q^2) \to dx_i d^2k_{T,i} g(\vec{k}_{T,i}) f_{i/p}(x_i, Q^2), \quad (2)$$

with $i = a, b$. In order to avoid singularities introduced by including partonic transverse momentum in the differential cross sections, describing the relevant subprocesses, we adopt the old-fashioned regularization scheme using a finite parton mass $m = 0.8$ GeV, as in [20,23,24], in the Mandelstam variables occurring in the denominator of the corresponding matrix elements as this choice is easier implemented in our phenomenological analysis. However, as it will be discussed below, the obtained numerical results are almost independent on the particular value of m.

The explicit formulas of the relevant partonic cross sections can be found in [22]. Taking into account the transverse degrees of freedom we get the following expressions for the variables $\hat{s}, \hat{t}, \hat{u}$:

$$\hat{s} = s x_a x_b + \frac{k_{T,a}^2 k_{T,b}^2}{s x_a x_b} - 2\vec{k}_{T,a} \cdot \vec{k}_{T,b},$$
$$\hat{t} = -\left(x_a + \frac{k_{T,a}^2}{s x_a}\right)\frac{p_T\sqrt{s}}{z_c} + \frac{2}{z_c}\vec{k}_{T,a} \cdot \vec{p}_T, \quad (3)$$
$$\hat{u} = -\left(x_b + \frac{k_{T,b}^2}{s x_b}\right)\frac{p_T\sqrt{s}}{z_c} + \frac{2}{z_c}\vec{k}_{T,b} \cdot \vec{p}_T.$$

Because of energy-momentum conservation the momentum fraction of the final hadron z_c is given by

$$z_c = \frac{(x_a + \frac{k_{T,a}^2}{s x_a} + x_b + \frac{k_{T,b}^2}{s x_b}) p_T\sqrt{s} - 2(\vec{k}_{T,a} + \vec{k}_{T,b}) \cdot \vec{p}_T}{\hat{s}}. \quad (4)$$

For a consistent description of the kinematics in the partonic subprocesses we imply the cuts:

$$z_c \le 1; \qquad k_{T,i}^2 < \min(p_T\sqrt{s}, x_i^2 s), \qquad i = a, b. \quad (5)$$

To calculate the cross section given in Eq. (1) we first have to determine the distribution $g(\vec{k}_T)$ and then perform the corresponding phase space integrations. Contrary to the usual treatment assuming a Gaussian form for $g(\vec{k}_T)$ we will here derive an alternative expression based on a widely applied quark potential model.

III. THE INTRINSIC TRANSVERSE MOMENTUM DISTRIBUTION $g(\vec{k}_T)$

Since the early days of quantum chromodynamics the main and almost unique tool used for the description of the hadronic bound states (mesons, baryons) remain potential models for the quark-quark and quark-antiquark pair interaction. One of the most successful models was proposed by A. Martin used first to describe mesonic states [28] and later to describe heavy baryons [30]. A similar model [34], with respect to its functional form, reproduces also the spectrum of light baryons. However, when short distance dynamics become relevant more realistic models including an explicit Coulomb part have been proposed by several authors [29,35]. In the following calculations we will use exclusively Martin's model [28,30] as we are less interested in a detailed description of the corresponding hadronic spectrum than in a rather rough estimation of bound state effects in the transverse momentum distribution of the partons inside the proton. The quark-quark interaction within this model is given as

$$V(r) = A_{qq} r^{0.1} + B_{qq}, \quad (6)$$

and a similar expression with adapted coefficients $A_{\bar{q}q}, B_{\bar{q}q}$ holds for the quark-antiquark interaction. In the following we will consider a baryon consisting of three valence quarks interacting pairwise with the potential (6). The Hamiltonian operator of the system is given as

$$\hat{H} = -\frac{\hbar^2}{2m}(\nabla_1^2 + \nabla_2^2 + \nabla_3^2) + V(\vec{r}_{12}) + V(\vec{r}_{23}) + V(\vec{r}_{31}). \tag{7}$$

The translation invariant part of the Hamiltonian (7) is searched for variationally as $\pi^{-3/2}\frac{u_0(\xi)}{\xi^{5/2}}$, with $\xi^2 = \frac{2}{3} \times (r_{12}^2 + r_{23}^2 + r_{31}^2)$, leading to [30]

$$\frac{d^2u_0}{d\xi^2} - \frac{15}{4\xi^2}u_0 + \frac{m}{\hbar^2}(E_G - \tilde{V}_{00})u_0 = 0, \tag{8}$$

where $\tilde{V}_{00} = A_{00} + B_{00}\xi^{0.1}$ with $A_{00} = \frac{3}{2}A_{qq}$ and $B_{00} = \frac{1}{2}\lambda B_{qq}$. The constant λ is given by $\lambda = \frac{24}{\pi}\Gamma(1.55)\Gamma(1.5)\Gamma(3.05)$. It is straightforward to show that the ground state wave function in the momentum space is given by

$$\tilde{\Phi}(k_\xi^2) = N\int_0^\infty d\xi\xi^{1/2}u_0(\xi)\frac{J_2(k_\xi\xi) - k_\xi\xi J_3(k_\xi\xi)}{k_\xi^2}, \tag{9}$$

where J_n is the Bessel function of order n and N is a normalization constant. In the center of mass frame ($\vec{k}_1 + \vec{k}_2 + \vec{k}_3 = \vec{0}$) of the baryonic system holds

$$k_\xi^2 = k_1^2 + k_2^2 + \vec{k}_1 \cdot \vec{k}_2,$$

and the two-particle density $\rho(\vec{k}_1, \vec{k}_2)$ is given by

$$\rho(\vec{k}_1, \vec{k}_2) = |\tilde{\Phi}(k_\xi^2)|^2 = |\tilde{\Phi}(k_1^2 + k_2^2 + \vec{k}_1 \cdot \vec{k}_2)|^2. \tag{10}$$

From Eq. (10) we obtain the one-particle transverse momentum density $g(\vec{k}_T)$ as

$$g(\vec{k}_T) = 4\pi\int_0^\infty dk_z\int_{-1}^1 dz\int_0^\infty dk_2k_2^2 \times \left|\tilde{\Phi}\left(k_T^2 + k_z^2 + k_2^2 + zk_2\sqrt{k_T^2 + k_z^2}\right)\right|^2, \tag{11}$$

where z is the cosine of the angle between the vectors $\vec{k} = (\vec{k}_T, k_z)$ and $\vec{k}_2$. In fact the function $u_0(\xi)$ can be obtained only numerically by solving Eq. (8) using the Numerov algorithm. Therefore the transverse momentum distribution (11) is also known only numerically. The integrations in Eqs. (9) and (11) can be performed to a great accuracy (relative error $\approx 10^{-6}$) using a mixture of Gauss-Kronrod quadrature and the VEGAS Monte-Carlo integration routine [36]. In Fig. 1 we present the density in transverse momentum space of a parton inside the proton obtained by our approach. The values of the constants A_{qq} and B_{qq} are chosen according to [30] in order to approximately fit the size and the binding energy of the proton. The characteristic structure of $g(\vec{k}_T)$ within our model is the second maximum at relative high transverse momenta. This leads, as we will see in the next section, to a reduction, relative to the Gaussian case, of the mean intrinsic transverse momentum of the partons needed to describe the experimental data for the π^0 production at various energies.

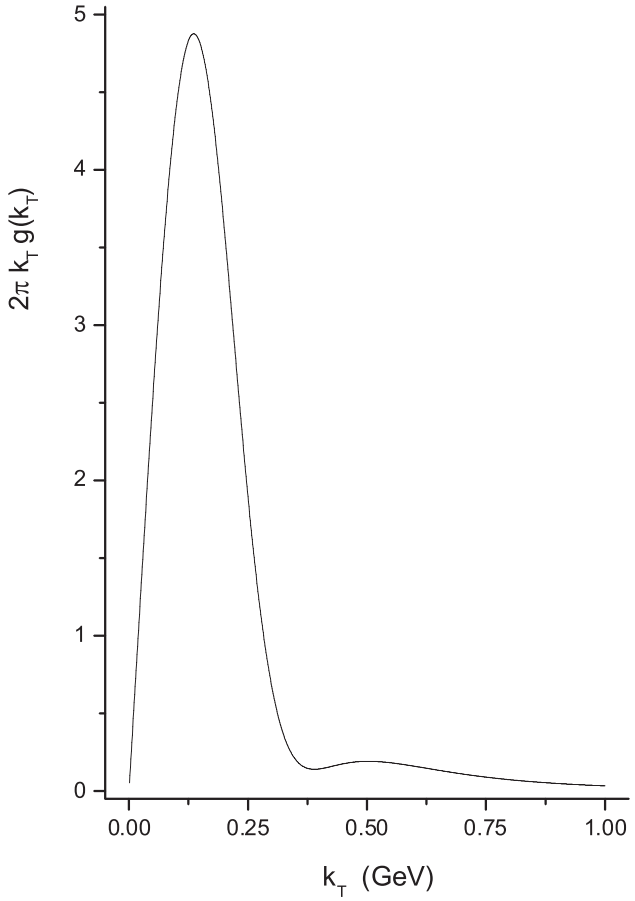

FIG. 1. The intrinsic transverse momentum distribution $2\pi k_T g(\vec{k}_T)$ of a parton inside the proton obtained through the quark potential model described in Sec. III.

IV. NUMERICAL RESULTS

In the following we will use the derived distribution $g(\vec{k}_T)$ in order to calculate within the parton model the differential cross section for the π^0 production in pp collisions according to Eq. (1). The only free parameter in our approach is the mean transverse momentum of the initial partons $\langle k_T \rangle$, related to the string tension B_{qq} in Eq. (6), which is adjusted in order to fit the experimental data for different beam energies and different transverse momenta p_T of the final hadrons. In addition, although the distribution $g(\vec{k}_T)$ is derived for the valence quarks inside the proton, here, we will use the same distribution also for the initial gluons assuming universality at the level of constituent partons. In any case for longitudinal momentum fraction $x_i > 0.5$ ($i = a, b$) the contribution of valence quarks is dominant and our description is accurate. The phase space integrations in Eq. (1) are performed using the VEGAS Monte Carlo routine.

As mentioned in [22] the values of the calculated cross sections are influenced by the choice of factorization scales Q, $\tilde{Q}$, the PDF, and FF and finally the inclusion or not,

through the K factor, of higher order corrections in the partonic subprocesses. In particular we are interested in estimating how the p_T dependence of the $\langle k_T \rangle$ values, needed for an accurate description of the experimental data, is affected by these choices. In order to proceed in a systematic way we consider four different sets, each one characterized by a particular choice of PDF, PFF, K facto,r and factorization scales Q, $\tilde{Q}$.

(1) In the first set we use for the PDF the recent Martin, Roberts, Stirling, and Thorne scheme [37] in next-to-next-to-leading order while for the PFF we use the Kniehl, Kramer, Potter [38] parametrization in next-to-leading order. For the partonic subprocesses we consider the leading order cross-sections with a $K = 2$ factor incorporating the higher order corrections. The factorization scales are fixed to $Q^2 = \tilde{Q}^2 = \frac{2\hat{s}\hat{t}\hat{u}}{\hat{s}^2+\hat{t}^2+\hat{u}^2}$ proposed in [20] with $\hat{s}$, $\hat{t}$, $\hat{u}$ the usual Mandelstam variables.

(2) In set 2 the PDF, PFF, and K factor are exactly the same as in set 1 while the corresponding choice for the factorization scales is $Q = p_T$ and $\tilde{Q} = \frac{p_T}{z_c}$.

(3) In set 3 we use the leading order Martin, Roberts, Stirling, and Thorne PDF [39], the leading order Kniehl, Kramer, Potter parametrization for the PFF, $K = 2$ and $Q^2 = \tilde{Q}^2 = \frac{2\hat{s}\hat{t}\hat{u}}{\hat{s}^2+\hat{t}^2+\hat{u}^2}$.

(4) Finally in set 4 we use the same choices as in set 3 but now we take $K = 1$ ignoring the effect of higher order corrections in the partonic subprocesses.

The detailed phenomenological analysis using all these sets in our numerical calculations is performed only for the most sensitive case in order to obtain an upper limit of $\langle k_T \rangle$. The remaining analysis is performed using exclusively set 1 which turns out to be the most representative with respect to the determined $\langle k_T \rangle$ values. Comparison between the results obtained using set 1 and set 2 allows us to estimate the effect of the factorization scales while the corresponding comparison between set 1 and set 3 isolates the influence of PDF and PFF choice in our calculations. Finally, comparing results obtained using set 3 and set 4, respectively, we extract the effect of the K factor.

We will analyze here the results of four experiments concerning π^0 production at different energies. The first set of data is taken from the fixed target experiment performed in Fermilab (protons incident on H_2 target) [1]. The cross section for the π^0 production with transverse momentum p_T at midrapidity and for three different proton beam energies $E_L = 200$, 300, and 400 GeV is measured. In Fig. 2 we present the various data sets using symbols while with solid lines we show the results of the calculation using the $g(\vec{k}_T)$ obtained in the previous section and with dashed lines the corresponding results using a Gaussian $g(\vec{k}_T)$. In both calculations we have chosen for PDF, PFF, K factor, and factorization scales Q, $\tilde{Q}$ those of set 1 described above. As we can see, the two descriptions differ only in the region $p_T < 1$ GeV. Within our approach we need an intrinsic transverse momentum $\langle k_T \rangle$ of the order of at most 0.5 GeV in order to reproduce all the experimental data. It must be noted that in this case one can perfectly fit the data also for $p_T < 1$ GeV which, as we clearly see in the inset of Fig. 2, is not possible using a Gaussian distribution $g(\vec{k}_T)$. In Fig. 3 we show the functions $\langle k_T \rangle (p_T)$ obtained using the quark model inspired function $g(\vec{k}_T)$ as well as a Gaussian form. These results correspond to the calculation presented in Fig. 2 and are obtained using set 1. It is evident that the Gaussian model leads to much higher values of $\langle k_T \rangle$. As already discussed in the previous section this difference relies on the fact that the non-Gaussian $g(\vec{k}_T)$ derived here possesses a second small local maximum at high transverse momenta (see Fig. 1) attributed to the form of the quark-quark potential and the many-body character of the system.

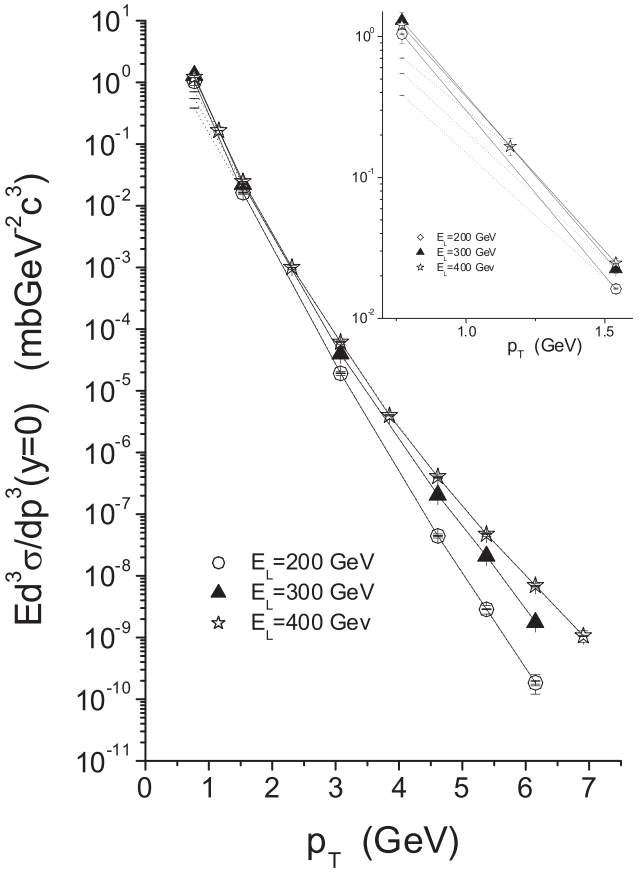

FIG. 2. The differential cross section for the π^0 production in the Fermilab experiment [1]. The symbols represent the experimental data sets for three different beam energies. The solid lines represent the parton model results using a non-Gaussian $g(\vec{k}_T)$ while the dotted lines correspond to the analogous results using a Gaussian k_T smearing. Only for $p_T < 1$ GeV the two fits differ. This is clearly displayed in the inset. For all the calculations we have used set 1 for PDF, PFF, K factor, and factorization scales Q, $\tilde{Q}$.

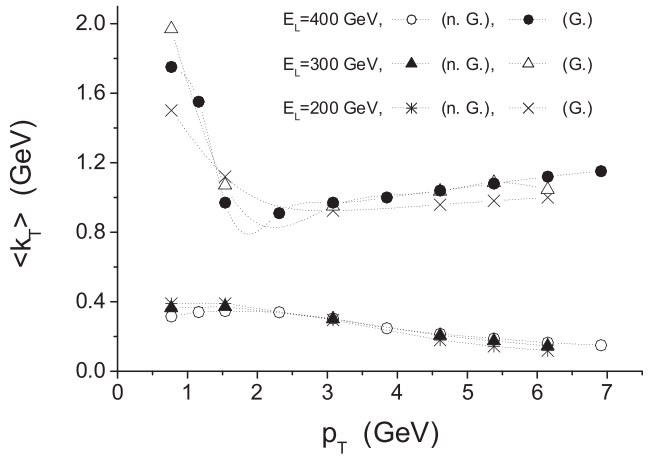

FIG. 3. The functions $\langle k_T(p_T)\rangle$ for the three data sets presented in Fig. 2. We distinguish between the results of the parton model using non-Gaussian (n. G.) or Gaussian (G.) intrinsic transverse momentum distribution.

As we can see in Fig. 3, the most sensitive process in the variation of $\langle k_T\rangle$ values is the π^0 production at $E_L = 200$ GeV. Therefore, we restrict to this process in order to perform a detailed phenomenological analysis of the p_T dependence of $\langle k_T\rangle$ using the four different sets of PDF, PFF, K factor, and factorization scales Q, $\tilde{Q}$ defined above and obtain an upper limit for the $\langle k_T\rangle$ values needed to describe the experimental data. In Fig. 4 we show the function $\langle k_T\rangle(p_T)$ for the four different choices: set 1 (open circles), set 2 (full triangles), set 3 (full stars), and set 4 (crosses). In all cases a perfect fit of the experimental data is achieved. We observe that the main variation of about 30% in the $\langle k_T\rangle$ value is caused by the choice of factorization scales Q, $\tilde{Q}$ (compare set 1 with set 2 results) and a similar effect ($\approx 26\%$) is induced by the choice of K factor (compare set 3 with set 4 results). The corresponding $\langle k_T\rangle$ variation caused by the choice of PDF and PFF is much smaller ($\approx 8\%$) (compare set 1 with set 3 results). Using set 4 we obtain the maximum value $\langle k_{T,max}\rangle \approx 0.53$ GeV needed to describe the π^0 production at $p_T = 0.77$ GeV and $E_L = 200$ GeV.

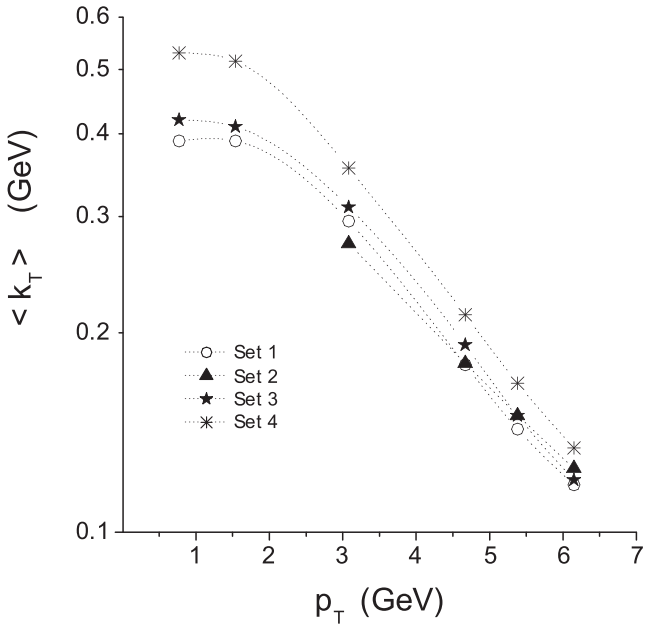

FIG. 4. The functions $\langle k_T(p_T)\rangle$ needed for a perfect fitting of the cross section for π^0 production at $E_L = 200$ GeV (CP Collaboration) using the different sets (1–4) of choices for PDF, PFF, K factor, and factorization scales Q, $\tilde{Q}$.

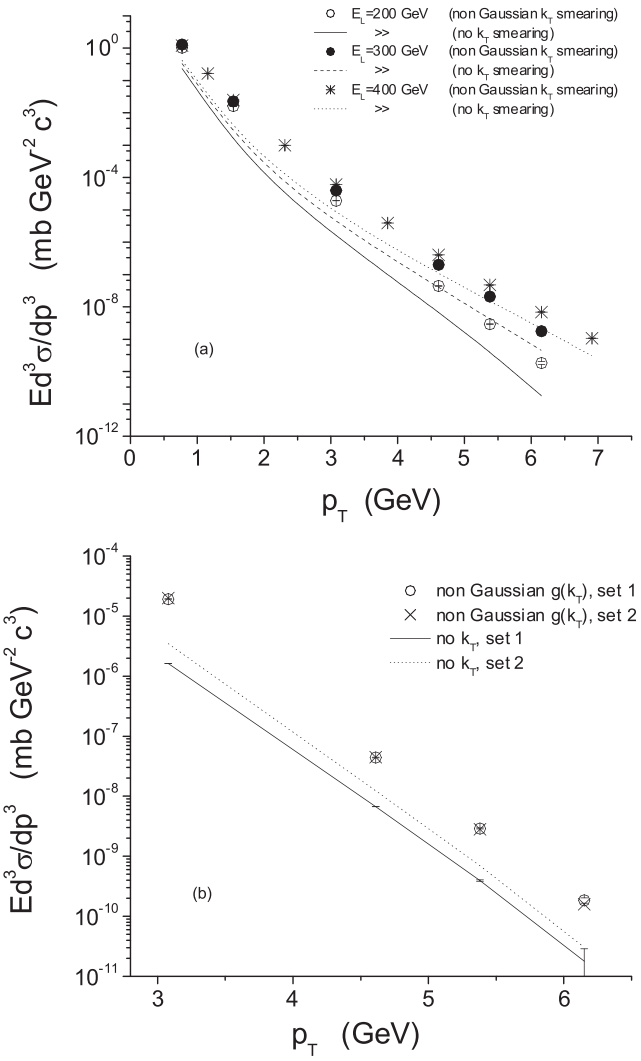

FIG. 5. (a) The differential cross section for the π^0 production in the Fermilab experiment [1]. The symbols represent the parton model results using a non-Gaussian $g(\vec{k}_T)$ while the lines correspond to the analogous results using the simple parton model without intrinsic transverse momentum. The PDF, PFF, K factor, and factorization scales Q, $\tilde{Q}$ are chosen according to set 1. (b) The differential cross section for π^0 production at $E_L = 200$ GeV using set 2 with (crosses) and without (dotted line) k_T smearing. For comparison we display also the corresponding results using set 1.

To estimate the contribution of the intrinsic partonic transverse momentum in the above calculations we have determined the cross sections for the π^0 production using the simple parton model without intrinsic transverse momentum distribution of the partons. In Fig. 5(a) we show the results of our calculations using set 1 for PDF, PFF, K factor, and Q, $\tilde{Q}$. With symbols we show the cross section obtained using non-Gaussian intrinsic transverse momentum distribution while with lines we give the corresponding results without intrinsic k_T. For the case of $E_L = 200$ GeV we have repeated the calculations using set 2. The results are displayed with crosses (including k_T smearing) and with a dotted line (no k_T smearing) in Fig. 5(b). In the same figure we also show for comparison the corresponding results using set 1 (open circles and solid line, respectively). It is clearly observed that the choice $Q^2 = \frac{2\hat{s}\hat{t}\hat{u}}{\hat{s}^2+\hat{t}^2+\hat{u}^2}$ is not the best in order to fit the experimental data by the simple (without intrinsic k_T) parton model. Therefore, the k_T-smearing effect shown in Fig. 5(a) is in fact overestimated. Here we are interested to show that using the non-Gaussian $g(k_T)$ the corresponding $\langle k_T \rangle$, needed to describe the experimental data, does not exceed the value compatible with Heisenberg's uncertainty relation. Therefore, in the following we will use the factorization scales given in set 1 obtaining in this way larger values for $\langle k_T \rangle$. On the other hand, we would like to argue that k_T smearing besides higher order corrections incorporates also nonperturbative effects and, therefore, we will use in the following calculations set 1 containing the most updated PDF and PFF and $K = 2$.

In order to test our model further, we also have calculated the cross section for $pp \to \frac{p+\bar{p}}{2} + X$ using the non-Gaussian transverse momentum distribution derived in the previous section and compared with the data available from the above mentioned CP Collaboration experiment at Fermilab [1]. The results are in very good agreement with those obtained from the π^0 production. In Fig. 6 we show the cross sections for the proton production at three different energies ($E_L = 200$, 300, and 400 GeV) as a function of the transverse momentum p_T of the final hadron. The experimental data are presented by symbols while the theoretical calculations are shown by solid lines. In Fig. 7 we display with symbols the $\langle k_T \rangle$ values used to obtain the theoretical results of Fig. 6 for different p_T. It is interesting that using values $\langle k_T \rangle < 0.55$ GeV we achieve a perfect description of the experimental data. In the same plot we present with solid lines the corresponding functions $\langle k_T \rangle(p_T)$ used to describe the π^0 production. The stratified area displays the range of $\langle k_T \rangle$ values needed for a good description of the π^0 production using Gaussian intrinsic transverse momentum distribution. Concerning the $\langle k_T \rangle$ dependence on p_T we observe a very good agreement of the results obtained from the π^0 production with those obtained from the proton production for $p_T > 4.5$ GeV.

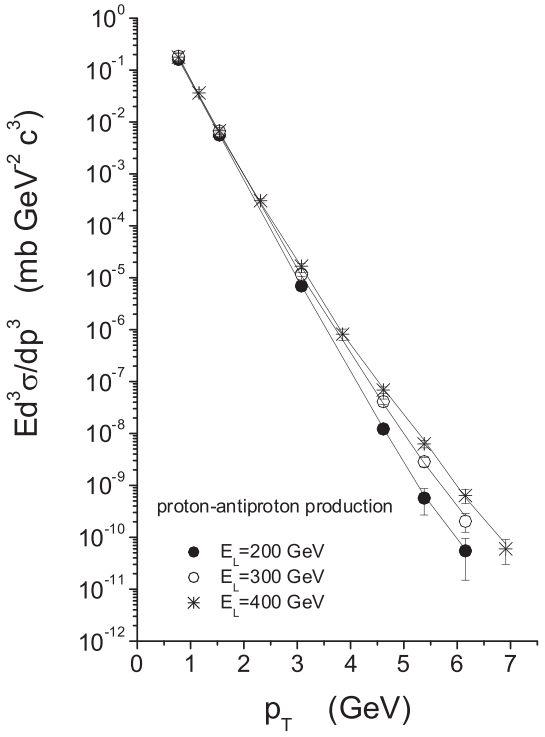

FIG. 6. The differential cross section for the $p + \bar{p}$ production in the Fermilab experiment [1]. The symbols represent the experimental data sets for three different beam energies. The solid lines represent the parton model results using a non-Gaussian $g(\vec{k}_T)$ (set 1).

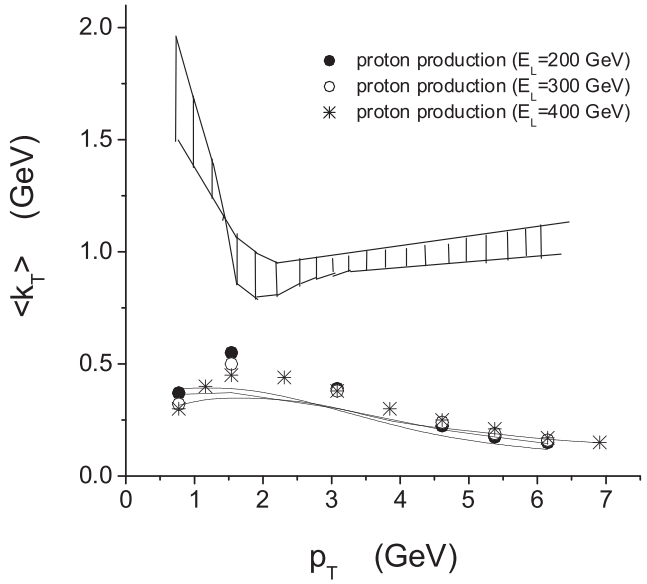

FIG. 7. The $\langle k_T \rangle$ values used to obtain the theoretical predictions of Fig. 6 (symbols). In the same plot we show the corresponding behavior obtained from the π^0 production. The stratisfied region determines the $\langle k_T \rangle$ domain needed to describe the π^0 production using Gaussian intrinsic transverse momentum distribution.

The second experiment we have considered is the π^0 production at the proton-proton Intersecting Storage Ring (CERN) [6]. We have calculated the cross section at two different energies $\sqrt{s} = 53$ and 63 GeV. Our results are shown in Figs. 8(a) and 8(b). As in the previous case in Fig. 8(a) we show the experimental data with symbols and with solid lines the theoretical results, using non-Gaussian k_T smearing, for the cross section $pp \to \pi^0 + X$ for different p_T values. In Fig. 8(b) we give the dependence $\langle k_T \rangle (p_T)$ used to obtain within our model the cross sections of Fig. 8(a). As one can see the needed values of $\langle k_T \rangle$ are in the range 0.18–0.23 GeV in accordance with the results obtained for the CP Collaboration.

The third experiment we consider is the WA70 at CERN SPS [7]. It is also a fixed target experiment with $E_L = 280$ GeV. We are interested in π^0 production. In Fig. 9 we show the experimental data (full stars) and the corresponding perturbative QCD calculation using the quark model inspired $g(\vec{k}_T)$ (solid line) as well as a Gaussian form (dashed line). In this p_T region both distributions reproduce perfectly the experimental data and cannot be distinguished graphically. However, our approach leads to significantly lower values of $\langle k_T \rangle$ than in the Gaussian case. This can be seen clearly in Fig. 10 where we show the function $\langle k_T(p_T) \rangle$ both for the quark potential model inspired $g(\vec{k}_T)$ (full circles) as well as the Gaussian intrinsic transverse momentum distribution (full stars). For comparison we present the same function for the Fermilab experiment at $E_L = 300$ GeV (open circles, see Fig. 3).

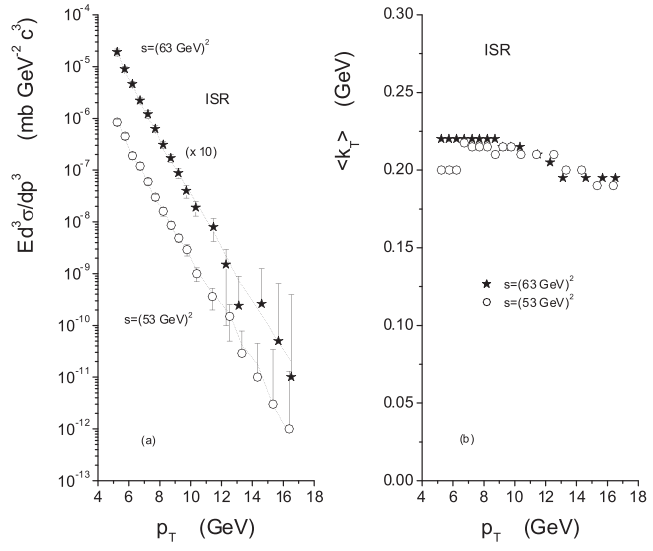

FIG. 8. (a) The differential cross section for the π^0 production in the ISR (CERN) experiment [6]. The symbols represent the experimental data sets for two different beam energies. The solid lines represent the parton model results using a non-Gaussian $g(\vec{k}_T)$ (set 1). (b) The $\langle k_T \rangle$ values (symbols) used to obtain the theoretical predictions of Fig. 8(a).

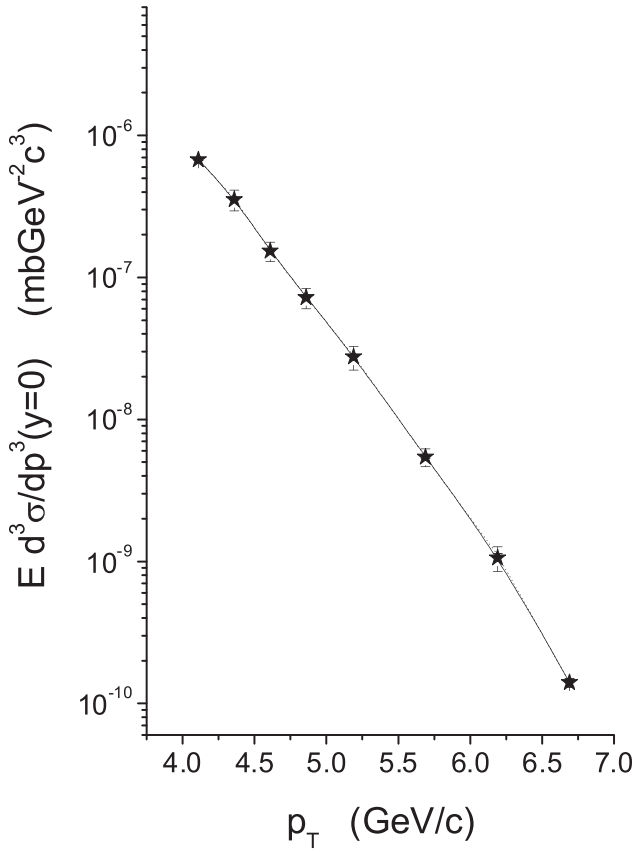

FIG. 9. The differential cross section for π^0 production in WA70 at $E_L = 280$ GeV (full stars) and the corresponding parton model calculation using a non-Gaussian (solid line) as well as a Gaussian (dotted line) $g(\vec{k}_T)$. Both distributions fit perfectly the experimental data in this p_T range and therefore are barely distinguishable in the present plot.

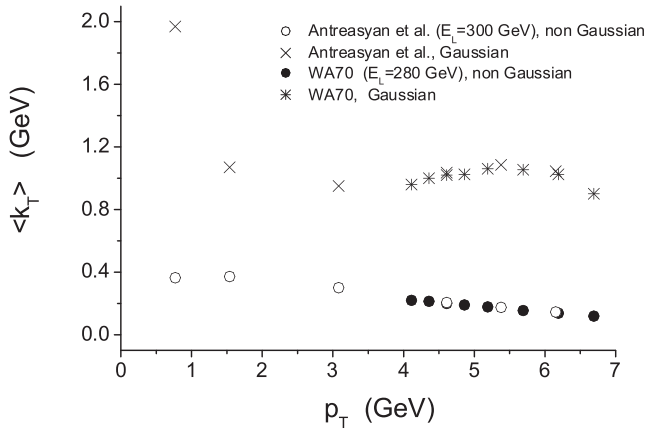

FIG. 10. The dependence $k_T(p_T)$ for the WA70 data set using a non-Gaussian as well as a Gaussian $g(\vec{k}_T)$ in comparison with the corresponding behavior found for the Fermilab experiment at $E_L = 300$ GeV with a non-Gaussian $g(\vec{k}_T)$.

Finally we have analyzed the $pp \to \pi^0 + X$ data of the most recent PHENIX experiment at the Relativistic Heavy Ion Collider with $\sqrt{s} = 200$ GeV [16]. The corresponding cross section can be described to a good accuracy without inclusion of any k_T smearing, a fact which is compatible with expectations for the perturbative character of the subprocesses involved in this case. Here we have fitted the experimental data using non-Gaussian k_T-smearing effects. In this way we get a perfect description of the measured cross section. The obtained mean intrinsic transverse momentum is almost constant: $\langle k_T \rangle \approx 250$ MeV. Based on Heisenberg uncertainty relation one could explain this value of the mean transverse momentum as an effect of the internal partonic structure of the incident proton. Our results are presented in Figs. 11 and 12. The PHENIX data (open cirlces) for $E\frac{d^3\sigma}{dp^3}$ together with the parton model calculations (crosses) using non-Gaussian $g(\vec{k}_T)$ are shown in Fig. 12. The corresponding function $\langle k_T \rangle (p_T)$ is presented in Fig. 12.

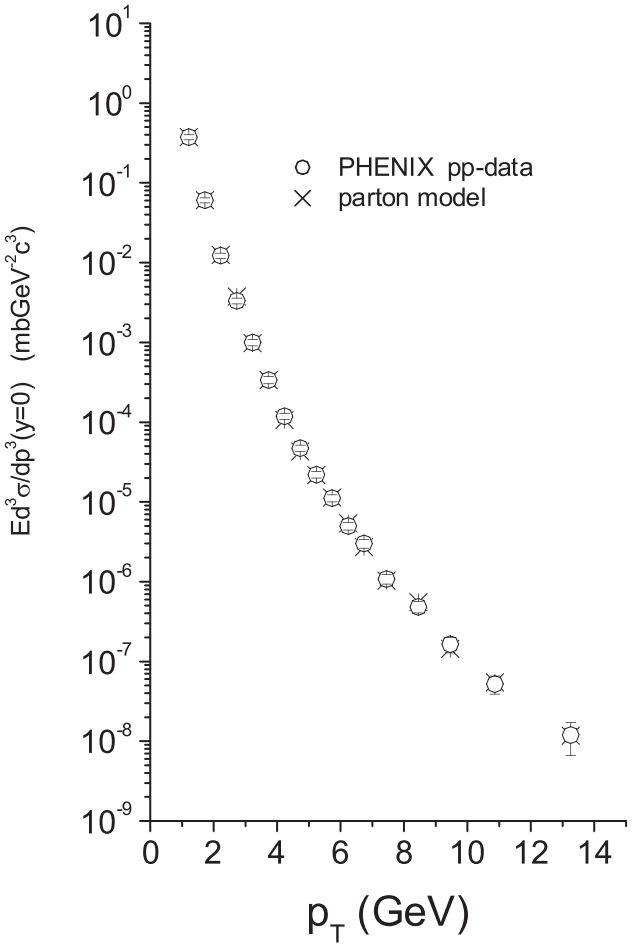

FIG. 11. The $pp \to \pi^0 + X$ differential cross section for the PHENIX experiment ($\sqrt{s} = 200$ GeV). The experimental data are presented by open circles while the crosses indicate the parton model calculation using a non-Gaussian k_T smearing (set 1). Only the experimental errors can be seen at this scale.

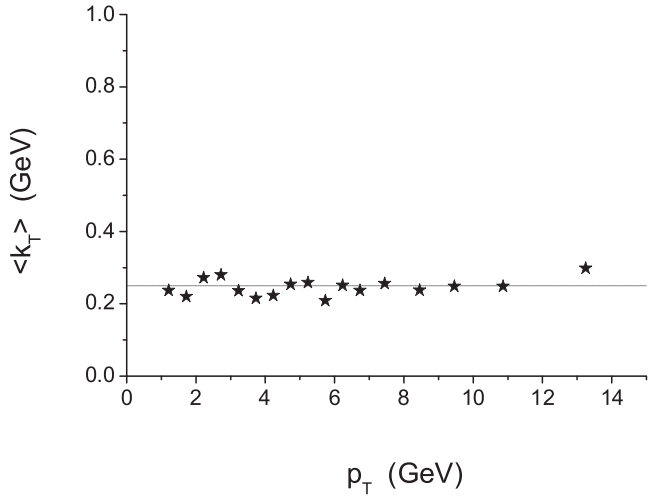

FIG. 12. The function $\langle k_T(p_T) \rangle$ obtained using the non-Gaussian $g(\vec{k}_T)$ in the parton model description of the PHENIX data. The solid line at 250 MeV is shown as a guide.

To allow for a good comparison between the Gaussian and non-Gaussian description of the intrinsic transverse momentum distribution of the partons we summarize all the results for the $\langle k_T(p_T) \rangle$ dependence, obtained through our analysis, in Fig. 13. We restrict ourselves to the results of the π^0 production. The Gaussian case concerns only the CP Collaboration data at the three energies ($E_L = 200$, 300, 400 GeV) and the corresponding $\langle k_T \rangle$ values are presented by the same symbol (full square) for all these energies. The non-Gaussian description determines a quite narrow band at relatively small values of $\langle k_T \rangle$ (compatible with the momentum uncertainty of the partons inside the

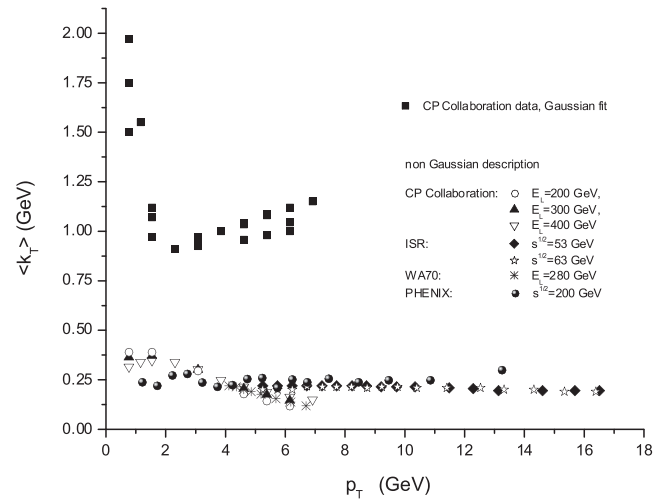

FIG. 13. The results for $\langle k_T(p_T) \rangle$ values obtained in order to describe the π^0 production data taking into account the intrinsic transverse momentum distribution of the partons.

proton) which suffices for a very good description of all the analyzed experimental data. Finally we would like to add a few comments concerning the parton mass introduced to regularize the singularities in the partonic cross sections after the introduction of k_T smearing. As already mentioned in Sec. II in all the presented results containing partonic transverse momenta we have used the value $m = 0.8$ GeV. In order to test the sensitivity of the obtained $\langle k_T \rangle$ on the choice of m we have performed calculations for π^0 production at $E_L = 200$ GeV (CP experiment) using different values of m varying from $m = 0.6$ GeV to $m = 1$ GeV. We have found that for low p_T the corresponding change in the $\langle k_T \rangle$ value was $\approx 5\%$ while for increasing p_T this variation decreases approaching 0 for $p_T = 6.15$ GeV. Thus the results presented above do not practically depend on the regularizing partonic mass m.

V. CONCLUDING REMARKS

Using a quark potential model capable to describe consistently baryonic systems as three quark bound states we have derived an intrinsic transverse momentum distribution $g(\vec{k}_T)$ of partons inside the proton. This, clearly non-Gaussian, distribution is characterized by the presence of a smooth local maximum at relatively high transverse momenta. Our approach is based on the idea that transverse momentum effects may be described nonrelativistically as they are not influenced by the Lorentz boost along the beam axis. Describing the k_T-smearing effects in the parton model for pp collisions through this non-Gaussian distribution we calculated the differential cross section for π^0 as well as p production at midrapidity for different beam energies. Assuming that the corresponding nonperturbative parameter $\langle k_T \rangle$, related to $g(\vec{k}_T)$, depends on p_T of the finally produced hadron as well as the incident energy, we obtain a very good description of the experimental data measured in pp collisions at four different experiments. The corresponding values of $\langle k_T \rangle$ as a function of p_T could originate, according to Heisenberg uncertainty relation, from the internal partonic structure of the proton and define a narrow band. It is interesting to investigate the possibility to describe in a similar way other processes like the single photon production, the Drell-Yan pair production or the deep inelastic scattering [40]. Additionally it is challenging to extend our approach to pA and AA processes. The performed analysis, although incorporating several approximations, shows that many-body effects through a confining potential, reflected at the level of one-particle distributions, may influence strongly the k_T-smearing phenomena observed in hadronic collisions and therefore should be taken into account for a better description of the experimental data.

ACKNOWLEDGMENTS

We thank N. G. Antoniou for helpful discussions. This work is financed by EPEAEK in the framework of PYTHAGORAS grants supporting university research groups under Contract No. 70/3/7420.

[1] D. Antreasyan *et al.*. (CP Collaboration), Phys. Rev. D **19**, 764 (1979).
[2] D. L. Adams *et al.* (E704 Collaboration), Phys. Lett. B **345**, 569 (1995); Phys. Rev. D **53**, 4747 (1996).
[3] C. De Marzo *et al.* (NA24 Collaboration), Phys. Rev. D **36**, 16 (1987).
[4] A. L. S. Angelis *et al.* (R110 Collaboration), Phys. Lett. B **185**, 213 (1987).
[5] D. E. Jaffe *et al.* (E605 Collaboration), Phys. Rev. D **40**, 2777 (1989).
[6] A. L. S. Angelis *et al.* (CCOR Collaboration) Phys. Lett. **79B**, 505 (1978); A. G. Clark *et al.* (CSZ Collaboration), Phys. Lett. **74B**, 267 (1978); C. Kourkoumelis *et al.*, Phys. Lett. **83B**, 257 (1979).
[7] M. Bonesini *et al.* (WA70 Collaboration), Z. Phys. C **38**, 371 (1988).
[8] T. Akesson *et al.* (R807/AFS Collaboration), Yad. Fiz. **51**, 1314 (1990) [Sov. J. Nucl. Phys. **51**, 836 (1990)].
[9] G. Ballocchi *et al.* (UA6 Collaboration), Phys. Lett. B **436**, 222 (1998).
[10] A. L. S. Angelis *et al.* (R108 Collaboration), Phys. Lett. **94B**, 106 (1980).
[11] A. L. S. Angelis *et al.* (R108 Collaboration), Nucl. Phys. **B327**, 541 (1989).
[12] E. Anassontzis *et al.* (R108 Collaboration), Z. Phys. C **13**, 277 (1982).
[13] D. M. Alde *et al.* (E772 Collaboration), Phys. Rev. Lett. **64**, 2479 (1990).
[14] M. J. Leitch *et al.* (E866 Collaboration), Phys. Rev. Lett. **84**, 3256 (2000).
[15] L. Apanasevich *et al.* (E706 Collaboration), Phys. Rev. Lett. **81**, 2642 (1998); Phys. Rev. D **59**, 074007 (1999).
[16] S. S. Adler *et al.* (PHENIX Collaboration), Phys. Rev. Lett. **91**, 241 803 (2003).
[17] R. D. Field, *Applications of Perturbative QCD*, Frontiers in Physics Lecture, Vol. 77 (Addison-Wesley, Reading, MA, 1989).
[18] J. Huston, E. Kovacs, S. Kuhlmann, H. L. Lai, J. F. Owens, and W. K. Tung, Phys. Rev. D **51**, 6139 (1995).
[19] M. Zieliński, hep-ph/9811278.
[20] R. P. Feynman, R. D. Field, and G. C. Fox, Phys. Rev. D **18**, 3320 (1978).
[21] D. Sivers, S. Brodsky, and R. Blankenbecler, Phys. Rep. **23**, 1 (1976); A. P. Contogouris, R. Gaskell, and S.

Papadopoulos, Phys. Rev. D **17**, 2314 (1978).
[22] J. F. Owens, Rev. Mod. Phys. **59**, 465 (1987).
[23] X. N. Wang, Phys. Rep. **280**, 287 (1997); Phys. Rev. Lett. **81**, 2655 (1998); Phys. Rev. C **58**, 2321 (1998).
[24] Y. Zhang, G. Fai, G. Papp, G. G. Barnaföldi, and P. Lévai, Phys. Rev. C **65**, 034903 (2002).
[25] X. Guo and J. Qiu, Phys. Rev. D **53**, 6144 (1996).
[26] H. L. Lai and H. N. Li, Phys. Rev. D **58**, 114020 (1998).
[27] G. Papp, P. Lévai, and G. Fai, Phys. Rev. C **61**, 021902(R) (2000).
[28] A. Martin, Phys. Lett. **100B**, 511 (1981).
[29] R. K. Bhaduri, L. E. Cohler, and Y. Nogami, Nuovo Cimento Soc. Ital. Fis. A **65**, 376 (1981).
[30] J. M. Richard, Phys. Lett. **100B**, 515 (1981).
[31] E. Cuervo-Reyes, M. Rigol, and J. Rubayo-Soneira, Rev. Bras. Ens. Fis. **25**, 18 (2003).
[32] R. K. Ellis, H. Georgi, M. Machacek, H. D. Politzer, and G. C. Ross, Phys. Lett. **78B**, 281 (1978); Nucl. Phys. **B152**, 285 (1979); S. Gupta and A. H. Mueller, Phys. Rev. D **20**, 118 (1979).
[33] R. P. Feynman, R. D. Field, and G. C. Fox, Nucl. Phys. **B128**, 1 (1977).
[34] J. M. Richard and P. Taxil, Phys. Lett. **128B**, 453 (1983); Ann. Phys. (N.Y.) **150**, 267 (1983).
[35] C. Roux and B. Silvestre-Brac, Few-Body Syst. **19**, 1 (1995).
[36] G. P. Lepage, J. Comput. Phys. **27**, 192 (1978).
[37] A. D. Martin, R. G. Roberts, W. J. Stirling, and R. S. Thorne, Phys. Lett. B **604**, 61 (2004).
[38] B. A. Kniehl, G. Kramer, and B. Potter, Nucl. Phys. **B582**, 514 (2000).
[39] A. D. Martin, R. G. Roberts, W. J. Stirling, and R. S Thorne, Phys. Lett. B **531**, 216 (2002).
[40] F. K. Diakonos, N. Kaplis, X. N. Maintas, and C. Papoulias (work in progress).